Pandal, A.; García-Oliver, JM.; Pastor Enguídanos, JM. (2020). Eulerian CFD modeling of nozzle geometry effects on ECN Sprays A and D: assessment and analysis. International Journal of Engine Research. 21(1):73-88. https://doi.org/10.1177/1468087419882500

Journal Title
XX(X):2–26

DOI: 10.1177/ToBeAssigned
www.sagepub.com/
SAGE

Eulerian CFD modeling of nozzle geometry effects on ECN Spray A and D: assessment and analysis

Adrian Pandal[1], Jose M. Garcia-Oliver[2] and Jose M. Pastor[2]

Abstract

Diesel spray modeling is a multi-scale problem with complex interactions between different flow regions, i.e. internal nozzle flow, near nozzle region and developed spray, including evaporation and combustion. There are several modeling approaches that have proven particularly useful for some spray regions although they have struggled at other areas, while Eulerian modeling has shown promise in dealing with all characteristics at a reasonable computational effort for engineering calculations. In this work the Σ-Y single-fluid diffuse interface model, based on scale separation assumptions at high Reynolds and Weber numbers, is used to simulate the Engine Combustion Network (ECN) sprays A and D within a RANS turbulence modeling approach. The study is divided into two parts. First of all, the larger diameter Spray D is modeled from the nozzle flow till evaporative spray conditions obtaining successful prediction of numerous spray metrics, paying special attention to the near nozzle region where spray dispersion and interfacial surface area can be validated against measurements conducted at the Advanced Photon Source at Argonne National Laboratory (ANL), including both the ultra-small-angle x-ray scattering (USAXS) and the x-ray radiography. Afterwards, an analysis of the modeling predictions is made in comparison with previous results obtained for the Spray A, considering the nozzle geometry effects in the modeling behaviour.

Keywords

Eulerian, Diesel spray, atomization, ECN, CFD, OpenFOAM®

Prepared using sagej.cls *[Version: 2017/01/17 v1.20]*

1 Introduction

Recent advanced combustion strategies, followed to reduce the high levels of NOx and particulate matter in direct injection compression ignition (CI) engines, increase the understanding necessity of the diesel spray formation process. Under these scenarios the fuel-air mixing formation, evaporation and subsequent combustion processes are related in a more complex way. Therefore, in order to achieve the desired high efficiency and emissions reduction, a special attention to the fuel injection process and the spray development must be devoted, with a major dependency on the injector characteristics and nozzle geometry [1–4].

Fuel injection transforms a high-speed liquid jet into a spray of fine droplets that quickly evaporate. Because of the extremely small length scales and high speeds, spray modeling is still a challenging task in which details of the atomization process remain obscure. Particularly, the characterization of the near-nozzle region composed by a short jet core of liquid phase with many wrinkles and ligaments is extremely difficult for both experimental and modeling investigations. This optically dense space within the first few millimeters of the injector is only penetrable with special diagnostics such as x-ray radiography [5–7]. In addition, due to the very high Reynolds and Weber numbers typical of fuel spray regimes, large density ratios, phase change, and often near-supercritical fluids [8], the complexity of the flow makes the direct numerical simulation of the dense spray region extremely expensive for engineering calculations.

At present, Lagrangian particle tracking is the favored approach for in-cylinder simulations due to reasons of computational cost. This kind of modeling approach treats the liquid phase using a Lagrangian reference frame and the gaseous phase using an Eulerian reference frame. Because of that, several primary atomization models have been developed; however, these models are not necessarily predictive, requiring inputs such as initial drop size and presenting an important lack of fidelity because nearly all existing drag, collision, breakup, and vaporization models are based on assumptions of near-spherical droplets in a sparse spray, which is an over-simplification in the dense spray region. An accurate representation of the fuel spray within an engine simulation is essential but the alternative interface capturing methods, which can resolve directly the interface evolution, require again extreme levels of computational effort [9]. Then, considering a coarser engineering mesh resolution where the interfacial details are far

[1]Departamento de Energía (Área de Mecánica de Fluidos), Universidad de Oviedo, Spain
[2]CMT-Motores Térmicos, Universitat Politècnica de València, Spain

Corresponding author:
Adrian Pandal, Departamento de Energía (Área de Mecánica de Fluidos), Universidad de Oviedo, 33203 Gijón (Asturias), Spain
Email: pandaladrian@uniovi.es

smaller than the mesh size, the smoothing features over the cells provide at the end a diffuse-interface treatment in an Eulerian framework.

In diffuse-interface Eulerian spray models, the unresolved interface features are modelled through the density of interfacial area, typically denoted by Sigma (Σ). These strictly Eulerian models, as the Σ-Y approach [10] emphasize the turbulent mixing of the gas and liquid, which is consistent with experimental observations in direct injection diesel sprays [11–13]. In addition, in-cylinder conditions for diesel fuel injection are supercritical or near-supercritical [8,14,15], the elevated temperatures and pressures result in very small surface tension forces and extremely high Weber numbers and then, the gas/liquid interface disappears and spray modeling becomes largely an exercise in modeling variable-density turbulent mixing. The interfacial area density, with dimensions of reciprocal length, represents how much interfacial area is present per unit of volume, being possible to predict drop size once the primary atomization process is complete. Therefore, diffuse-interface Eulerian approaches seem to have both numerical (reduced computational effort, possibility to directly include internal nozzle flow in the spray simulation) and physical advantages, producing recent good results [16–25] and their popularity is increasing because with the diminishing cost of computational resources. Eulerian spray modeling has potential for being applied to engine development in the near future offering a more real representation as well as the injector/spray coupling capability.

However, in contrast to the liquid dispersion modeling, the surface quantity presents several unclosed terms and due to that different modeling approaches have been explored to solve them [16,26,27]. This clearly highlights the fact that experimental collaboration is needed to improve modeling performance. The Engine Combustion Network (ECN) [28] was created to allow this collaboration among experimental and computational researchers in engine combustion and thus, in its framework the present research work has been developed.

In the present paper, the fully Eulerian Σ-Y model [19], implemented in the OpenFOAM CFD open source c++ library [29], is evaluated to simulate diesel engine-like conditions against experimental measurements of ECN sprays A and D. In first term, the investigation is focused on modeling the more recent Spray D, including in-nozzle and external flow variables, spray structure in the near-nozzle region, interfacial surface predictions and vaporizing spray effectiveness. After that, modeling predictions are analysed in comparison with previous results obtained for the Spray A in order to understand the effects of the injector nozzle geometry in the modeling behaviour.

2 Σ-Y model description

The Σ-Y model considers the liquid/gas mixture of a spray as a pseudo-fluid with a single velocity field. In the case of direct injection Diesel sprays, the flow exiting the injector is operating at large Reynolds and Weber numbers. Thus, it is possible to consider a separation of the large scale flow features, such as mass transport, from the atomization process occurring at smaller scales. This allows the simulation of the large scale bulk

transport of the liquid, while unresolved turbulent transport is modelled using standard closures such as those used in Reynolds-averaged turbulence models.

To track the dispersion of the liquid phase an indicator function is used, taking a value of unity in the liquid phase and zero in the gas phase. The mean liquid volume fraction is denoted ($\overline{Y}$) and the mean mass averaged fraction is defined as ($\tilde{Y} = \frac{\overline{\rho Y}}{\bar{\rho}}$). Favre averaging the transport equation for the liquid mass fraction yields Eq. (1)

$$\frac{\partial \bar{\rho}\tilde{Y}}{\partial t} + \frac{\partial \bar{\rho}\tilde{u}_i\tilde{Y}}{\partial x_i} = -\frac{\partial \bar{\rho}\widetilde{u'_i Y'}}{\partial x_i} - S_{evap} \tag{1}$$

where u' denotes the density weighted turbulent fluctuations in velocity and Y' denotes turbulent fluctuations in liquid mass fraction and S_{evap} the evaporation source term. The turbulent diffusion liquid flux term, $\widetilde{u'_i Y'}$, captures the effect of the relative velocity between the two phases[10]. This term is modelled using a standard turbulent gradient flux model, which worked successfully for Diesel spray compared to DNS results, as indicated in [16].

$$\bar{\rho}\widetilde{u'_i Y'} = -\frac{\mu_t}{Sc}\frac{\partial \tilde{Y}}{\partial x_i} \tag{2}$$

where μ_t is the turbulent viscosity and Sc is the Schmidt number which will take the value of 0.9 as in other previous works[17–19,21,22].

Under the assumption that the two phases form an immiscible mixture, the mass-averaged value of the indicator function is related to the density by:

$$\frac{1}{\bar{\rho}} = \frac{\tilde{Y}}{\rho_l} + \frac{1-\tilde{Y}}{\rho_g} \tag{3}$$

then an equation of state is assigned to each phase to calculate the corresponding densities. The mixture of gas phases obeys an ideal gas law, while for the liquid phase, density is calculated following the Hankinson-Brobst-Thomson (HBT) correlation[30], in which the liquid density is a function of temperature (T) and pressure (p).

In order to account for spray evaporation, both an additional transport equation for vapor fuel mass fraction and also a procedure for calculating the source term, S_{evap}, of Equation 1 have to be added. The transport equation can be written in a similar way to the conservation of liquid fuel as:

$$\frac{\partial \bar{\rho}\tilde{Y}_v}{\partial t} + \frac{\partial \bar{\rho}\tilde{u}_i\tilde{Y}_v}{\partial x_i} = -\frac{\partial \bar{\rho}\widetilde{u'_i Y v'}}{\partial x_i} + S_{evap} \tag{4}$$

Again the standard turbulent gradient law is used for closure in this transport equation. This sink/source terms for fuel liquid/vapor transport equations are calculated in terms of a rate needed to achieve the local adiabatic saturation conditions. This can be written as

$$S_{evap} = \bar{\rho}\frac{Y_{v,sat} - \tilde{Y}_v}{\tau_{evap}} \tag{5}$$

where $\tilde{Y}_v$ is the local vapor fuel mass fraction, $Y_{v,sat}$ is the value of vapor fuel mass fraction under adiabatic saturation conditions and τ_{evap} is a relaxation time set equal to the computational time step. Finally, $Y_{v,sat}$ is calculated by means of a Locally Homogeneous Flow (LHF) approach[31], considering the mixing-controlled assumption[12]. According to that, state relationships are applied to describe spray thermodynamic conditions under the assumption of local thermodynamic equilibrium.

To close the above system of equations, the temperature is obtained from a bulk mixture enthalpy equation, under the assumption of local thermodynamic equilibrium:

$$\begin{aligned} h\left(T\right) &= Z \cdot h_f\left(T_0\right) + \left(1 - Z\right) \cdot h_a\left(T_a\right) \\ &= \tilde{Y} \cdot h_{f,l}\left(T\right) + \tilde{Y}_v \cdot h_{f,v}\left(T\right) \\ &+ \left(1 - \tilde{Y} - \tilde{Y}_v\right) \cdot h_a\left(T\right) \end{aligned} \tag{6}$$

where $Z = \tilde{Y}_v + \tilde{Y}_v$ is the mixture fraction. $h_{f,l}$, $h_{f,v}$ and h_a denote the enthalpy of the liquid and vapor fuel and the ambient gas phase, respectively. For the vapor fuel and the ambient gas, enthalpies are derived from the respective specific heat capacities at constant pressure evaluated from 7-coefficients NASA polynomials. After that, for the liquid fuel the enthalpy of vaporization ΔH_v is considered, as obtained from the corresponding states correlation by Pitzer et al.[32].

Finally, being h the static enthalpy implemented through the following conservation equation, where α_{eff} is the effective turbulent thermal diffusivity and $\tau_{ij}\frac{\partial u_j}{\partial x_i}$ the viscous dissipation:

$$\frac{\partial \bar{\rho} h}{\partial t} + \frac{\partial \bar{\rho} \tilde{u}_i h}{\partial x_i} - \frac{\partial}{\partial x_i}\left(\alpha_{eff}\frac{\partial h}{\partial x_i}\right) = \frac{\partial p}{\partial t} + u_i\frac{\partial p}{\partial x_i} + \tau_{ij}\frac{\partial u_j}{\partial x_i} \tag{7}$$

The solution of the preceding equations fully characterizes the large-scale bulk motion of the flow. As a result of the separation of scales, atomization is modelled by solving a transport equation for the evolution of the interface surface area density Σ, which is defined as the liquid surface present per unit volume at a given time and spatial position. Following the equation adopted by Vallet and Borghi[33], in which nearly all the models in the literature are based, the subsequent transport equation for Σ reads as shown in Eq. 8, which assumes a gradient law closure for the turbulent diffusion flux term.

$$\frac{\partial \tilde{\Sigma}}{\partial t} + \frac{\partial \tilde{u}_j \tilde{\Sigma}}{\partial x_j} - \frac{\partial}{\partial x_j}\left(D_\Sigma \frac{\partial \tilde{\Sigma}}{\partial x_j}\right) = C_\Sigma \tilde{\Sigma}\left(1 - \frac{\tilde{\Sigma}}{\bar{\Sigma}_{eq}}\right) + S_{\Sigma_{evap}} + S_{\Sigma_{init}} \tag{8}$$

$$C_\Sigma = \alpha_1 \frac{\tilde{\varepsilon}}{\tilde{k}} \tag{9}$$

$$\bar{\Sigma}_{eq} = \alpha_2 \frac{(\rho_l + \rho_g)\bar{Y}(1-\bar{Y})\tilde{k}}{\sigma} \tag{10}$$

where D_Σ is a suitable diffusion coefficient usually taken as the turbulent viscosity (ν_t) over a Schmidt number (Sc_Σ). The $S_{\Sigma_{evap}}$ term appears because of the change in the interface surface as a result of fuel evaporation and is modelled as in Lebas et al.[34]. C_Σ is an inverse time scale while $\bar{\Sigma}_{eq}$ is the equilibrium or critical surface density to which the local surface density is driven, quantities modelled as in Duret et al.[35]. Note the presence of the two modeling constants at these terms, α_1 and α_2, respectively. While the first one is directly a constant which smoothly drives the computed Σ towards the equilibrium value, the second one is inversely proportional to the critical Weber number (We_c) defined by Duret et al.[35]. Finally, the $S_{\Sigma_{init}}$ term is a proper initialization source term, which is necessary due to the fact that all the terms involved in the equation are proportional to the interface surface density (Σ). A detailed explanation of the terms in Eq.(8) together with the numerical implementation of this solver can be found in[17–19,21–23,27].

3 Experimental data

In this study, Σ-Y model assessment to simulate diesel sprays is made through the non-cavitating single-hole ECN database[6,28,36,37]. A tomographic reconstruction of both injection nozzles used in this work is depicted in Fig. 1. Here, one can observe the offset of the orifice outlet with respect to the needle axis present in the case of Spray A injector. This is considered and discussed at next section (Sec. 4) in order to generate the computational meshes. Detailed internal nozzle geometric and hydraulic characterization has been performed for the injectors employed in these experiments[38–40], being the main characteristics presented in Table 1. This includes the nozzle orifice outlet diameter, D_o, the steady state values of momentum and mass fluxes as well as the dimensionless coefficients, velocity coefficient, C_v, discharge coefficient, C_d, and area coefficient, C_a.

Table 1. Nozzle characteristics for single-hole non-cavitating ECN injectors.

Injector	$D_o[\mu m]$	$\dot{m}$[g/s]	M[N]	C_v[-]	C_d[-]	C_a[-]
Spray A #210675	89.4	2.56	1.52	0.918	0.9	0.98
Spray D #209133	180	11.71	6.82	0.907	0.885	0.975

The ECN database features a collection of experimental data of a free diesel spray injected into a quiescent environment, where well-defined boundary conditions are available for model validation purposes. Although the nominal condition for these sprays corresponds to 150 MPa injection pressure, 900 K ambient temperature and 22.8 kg/m^3 as ambient density, in a first step, the standard non-evaporating cold condition of ECN is used in order to evaluate the model in terms of the near-field structure (dense region) of diesel sprays, taking advantage of the valuable x-ray radiography measurements available at ECN database. This experiment is conducted with the ambient gas at room temperature (303 K) due to the x-ray transparent polymer windows used, which cannot

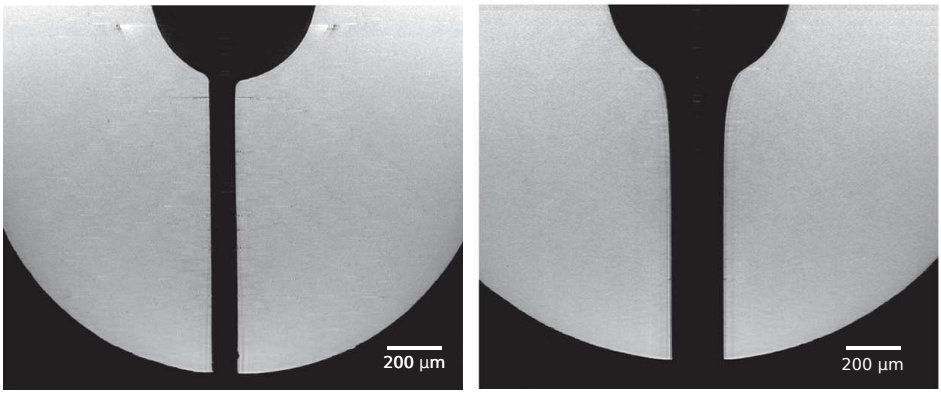

Figure 1. Tomographic reconstruction of (a) Spray A and (b) Spray D ECN single nozzle injectors[39]

Table 2. Conditions for standard non-vaporizing conditions ECN experiment.

Fuel	*n*-Dodecane
Ambient composition	100% N2
Injection pressure [MPa]	150
Ambient temperature [K]	303
Ambient density [kg/m^3]	22.8
Fuel injection temperature [K]	343

be used at high temperature. Nevertheless, the same ambient density of the nominal evaporating spray condition is matched in order to reproduce similar conditions for the spray breakup process, assuming that density is a more critical parameter than pressure for atomization[41]. The main conditions of this experiment are presented in Table 2. Further details about the experimental set-up are provided in[5].

The experimental data used for validation include useful quantities obtained from the x-ray radiography measurements conducted at the Argonne National Laboratory (ANL) namely the projected mass density (PMD) of the fuel, which is calculated by a line-of-sight integration along the x-ray beam[5,7] and the transverse integrated mass (TIM), which is obtained from the integral of the projected density across the transverse position at a particular axial location[6]. Additionally, measurements of spray surface area[42] (in terms of surface area per unit area of the x-ray beam) made using ultra-small angle x-ray scattering (USAXS) technique[37], have been used in order to evaluate Σ model predictions. This diagnostic technique provides quantitative information about the complex interface without resorting to the assumption that the liquid is in the form of droplets.

Finally, in the case of ECN Spray D an evaluation of model predictions is made under vaporizing conditions. The nominal condition (150 MPa, 900 K and 22.8 kg/m^3) is simulated together with a set of parametric variations based on this reference case.

This includes lower and higher injection pressure (DP1 and DP2) and ambient density conditions (DD1 and DD2), and reductions in ambient temperature (DT1 and DT2), as can be seen in Table 3. Model performance is characterized by means of a typical global spray parameter such as liquid and vapor tip penetration and compared against the proper experimental measurements[36].

Table 3. Simulated Spray D parametric variations studies under vaporizing conditions

Spray D condition	$\mathbf{P_{inj}}$[MPa]	T_{amb}[K]	ρ_{amb}[kg/m^3]
Baseline	150	900	22.8
DP1	**50**	900	22.8
DP2	**100**	900	22.8
DD1	150	900	**15.2**
DD2	150	900	**35.0**
DT1	150	**700**	22.8
DT2	150	**800**	22.8

4 Computational Domain and Model set-up

In order to conduct present investigation, some of the conclusions presented by Desantes et al.[18] will be used as initial set-up. As is widely known, nozzle geometric parameters have a great impact on the spray behavior. Thus, including nozzle effects by coupling internal and external flow simulations leads to a better representation of reality, specially in the case of the Spray A due to the misalign of the orifice with respect to the injector axis. The effect of this particularity has been studied in[18]. In this work was shown that a 3D internal nozzle flow simulation is able to capture the impact of the nozzle asymmetry in the internal structure of a diesel spray at the near-field. However, even more important, it was exposed that nozzle influence vanishes downsteam (around 6 mm) and 2D and 3D simulations show an almost identical performance, with an important computational cost reduction in the case of the 2D computational domain. For this reason, in this work only 2D simulations are conducted.

Additionally, in the case of the 2D simulations it was proven that internal and external flow calculations can be performed independently, which allows to feed the inlet boundary condition of an external flow simulation with the fields obtained at the nozzle exit in a coupled internal/external flow study, keeping in this way the effect of the nozzle profiles on the flow at a reduced computational cost. Then, two different 2D axisymmetric computational domain constructions are used in this work. First of all, the meshes including the nozzle geometry together with a spray chamber of 12 mm in length and 14 mm in diameter are considered to model a free fuel jet, one for each injector type. In Fig. 2a, the mesh structure can also be seen. These meshes were built after performing a grid sensitivity analysis which provides and optimum mesh with a minimum cell size of around 1.5 μm near the walls at the orifice outlet and a maximum cell size of 300 μm

far from the orifice exit. These simulations used a static mesh with the needle positioned at maximum lift.

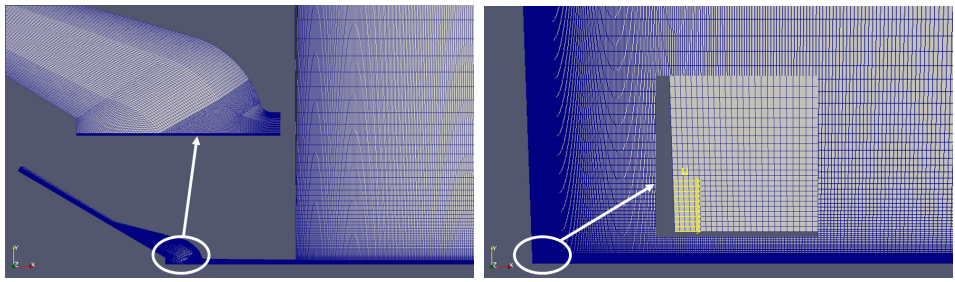

(a) Grid construction used for coupled nozzle-spray simulations

(b) Grid construction used for de-coupled spray simulations

Figure 2. Computational grids for ECN single nozzle spray simulations

Finally, in order to simulate a fully developed spray (external flow), a 2D axisymmetric computational domain without the nozzle geometry is considered corresponding to a cylindrical spray chamber of 108 mm in length and 50 mm in diameter. A structured mesh with non-uniform grid resolution is constructed. It consists of more than 60 thousand hexahedral cells, with an expansion ratio of 1.01 and 1.06 in the axial and radial directions, respectively, as indicated in [19], keeping an aspect ratio close to one in the near nozzle region, as depicted in Fig. 2b.

The proposed methodology allows to divide the problem reducing the computational effort, see Table 4, due to the fact that the internal flow domain (with smaller cells) is only solved till near-nozzle region (a fully developed spray in a domain that includes the nozzle geometry would require more than 144 hours) and then, the fully developed spray is conducted in an exclusive external flow domain with larger cells. As stated at [18], the fact of using the same solver for the resolution of both domains makes almost no differences in the results. On the other hand, in order to feed the external flow domain with the profiles obtained at the nozzle exit of the internal flow simulation, an interpolation from smaller cells to the bigger ones should be made. To do that, the mapped boundary condition of OpenFOAM is used to impose velocity, turbulence, density and temperature profiles. Regarding boundaries, the computational domain is opened at both the top and final ends of the mesh, while a symmetry boundary condition is chosen for both side planes. Regarding the wall located above the inlet, a no-slip condition was selected. A non-reflexive boundary condition is used for the opened outlet and two different options are used for the inlet depending on the mesh. In this regard, coupled domain simulation is made with a constant pressure profile as inlet boundary condition while, as previously discussed, the fields obtained at the nozzle exit in the coupled simulation were used as inlet boundary condition for the de-coupled one (only external flow), but properly scaled according to the injection mass flow rate [38,40].

Table 4. Computational cost comparison between different simulations

Simulation type	Wall clock time (hours)	Number of CPU
2D coupled	72	8
2D decoupled	56	8

The k-ϵ turbulence model was employed for the simulations. Due to the well known round jet spreading overprediction of k-ϵ type models[43], a corrected value for $C_{1\epsilon} = 1.60$ is used, as suggested by Pope[43] for round jets, and also used in other works[17,18,21,23]. Numerically, the discretization of the divergence terms was solved with a Gamma NVD scheme and a first order Euler scheme was applied for time derivative terms.

5 Results and Discussion

5.1 Nozzle and spray flow under standard non-vaporizing conditions

Table 5 summarizes momentum and mass fluxes for Spray D at the nozzle exit for the non-vaporizing condition to prove the model performance for in-nozzle simulations. Then, non-dimensional flow coefficients are calculated from such results and all these values are compared against experimental measurements. At the sight of the results, model predicts values with an error lower than 4% with respect to experimental ones, in line with results reported for Spray A[22], this fact encourages to continue with the stablished plan and conduct Spray D internal flow simulation for the injection pressure variations cases (100 and 50 MPa), in this manner the needed boundary conditions for the vaporizing simulations are provided.

Table 5. Steady state parameters (mass flow rate-$\dot{m}$ and momentum-$\dot{M}$) and non-dimensional flow coefficients (velocity coefficient-C_v, area coefficient-C_a and discharge coefficient-C_d).

	$\dot{m}$[g/s]	M[N]	C_v[-]	C_d[-]	C_a[-]
Experimental	11.71	6.82	0.907	0.885	0.975
CFD simulation	11.27	6.60	0.909	0.903	0.993
Relative Error (%)	3.84	3.21	0.22	2.02	1.87

Projected Mass Density (PMD) data has been used in order to evaluate liquid spray dispersion calculations in the near-nozzle region. Line-of-sight integration has been applied to predicted fuel density in order to replicate x-ray radiography measurements[42,44]. In Fig. 3 measured and predicted PMD contours are presented, showing that the simulations capture the spray fuel distribution in the near-nozzle region.

Then, more detailed comparison can be made by comparisons at the transverse direction for different axial positions ($0.1\ mm$, $2.0\ mm$, and $6.0\ mm$) downstream of the nozzle exit, as shown in Fig. 4. This figure shows the profiles of the 2D coupled simulation (as reference) against the profiles achieved with the decoupled one and regarding the experimental measurements, it should be noted that profiles have been centered about the Full Width at Half Maximum (FWHM) to allow a better comparison

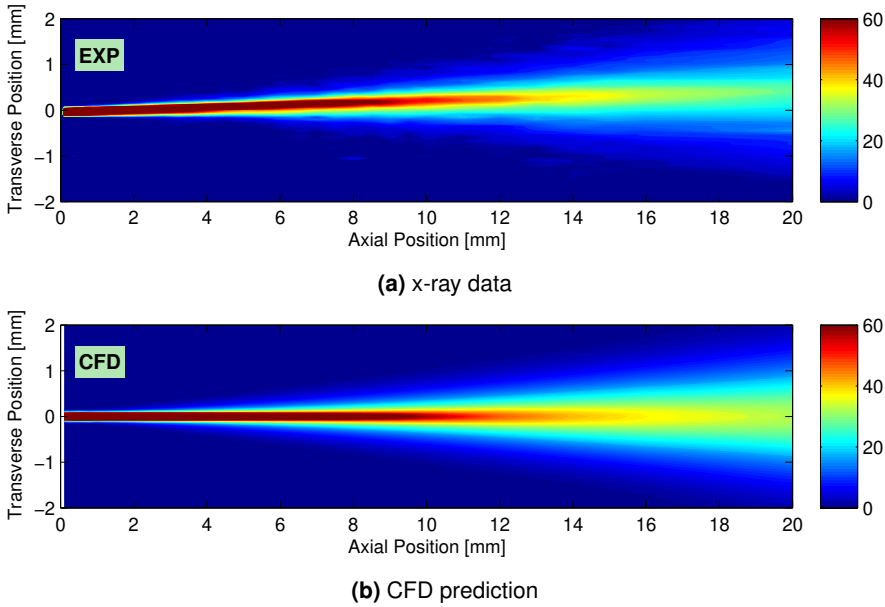

(a) x-ray data

(b) CFD prediction

Figure 3. Projected mass density [μg/mm^2] distributions at 725 μs after SOI

with axisymmetric simulations. Comparing CFD predictions with the experimental measurements, in general both the peak projected density at the spray centerline and the radial dispersion are well captured. However, a slightly overpredicted peak value is shown at the axial location of 6 mm downstream. Focusing the attention on the modeling, both provide quite similar results with a minor difference in terms of peak projected density. This is something expected, model ability to perform internal and external flow calculations independently was shown in Desantes et al.[18] work and here has been ensured with the Spray D reference case. For this reason, a brief comparison between coupled/decoupled results is made in this work.

Additionally, the axial transverse integrated mass (TIM), which quantifies the amount of liquid fuel mass present per unit legth in the axial direction and is obtained from the integral of the projected density across the transverse position at a particular axial location[6], is depicted in Fig. 5. Once again, quite similar results are provided by the simulations and an extremely good agreement is shown in comparison with the x-ray data within the first 10 mm downstream of the nozzle exit. As TIM is inversely proportional to the mass-averaged axial spray velocity, this result indicates that model can capture fairly well the liquid fuel axial velocity in the near-nozzle region. As a result, decoupled simulation is used for the following studies including full-spray development.

Finally, in order to close the study under non-vaporizing conditions, interface surface area density predictions are evaluated in comparison with USAXS results[42] used for

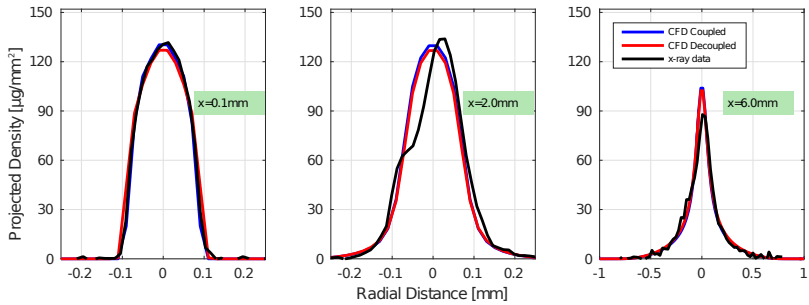

Figure 4. Computed and measured profiles of projected mass density [μg/mm^2] at 725 μs after SOI at axial locations of 0.1 mm, 2.0 mm, and 6.0 mm downstream of the nozzle exit

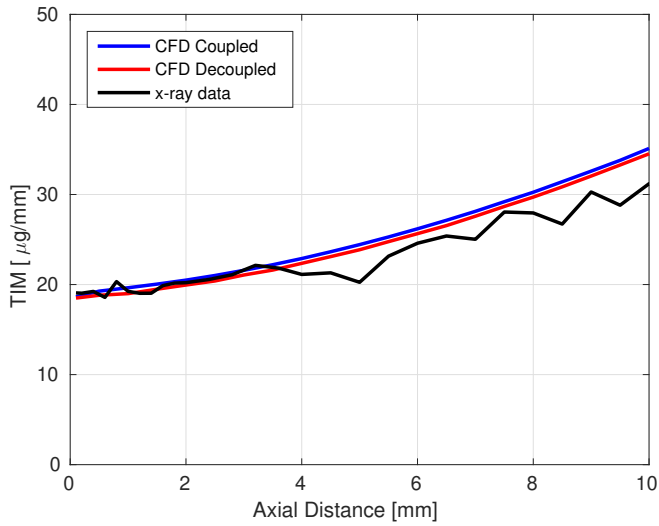

Figure 5. Computed and measured profiles of transverse integrated mass along the axis at 725 μs after SOI

spray atomization characterization. This experimental surface area is likewise line-of-sight integrated so CFD predictions must be processed to allow a fair comparison. The interface surface area density (Σ) value within each CFD cell is integrated through the depth of the spray, collapsing the surface area to a 2D map (it should be noted that for 2D computations, axisymmetry is assumed).

An example of model predictions of Σ is presented in Fig. 6. It can be observed that interface production starts after the spray core and peaks downstream, being less dense at the axis till around 6 mm due to the presence of the liquid intact core. This provides a double peak radial profile shape as shown later in Fig. 7. In order to compute surface

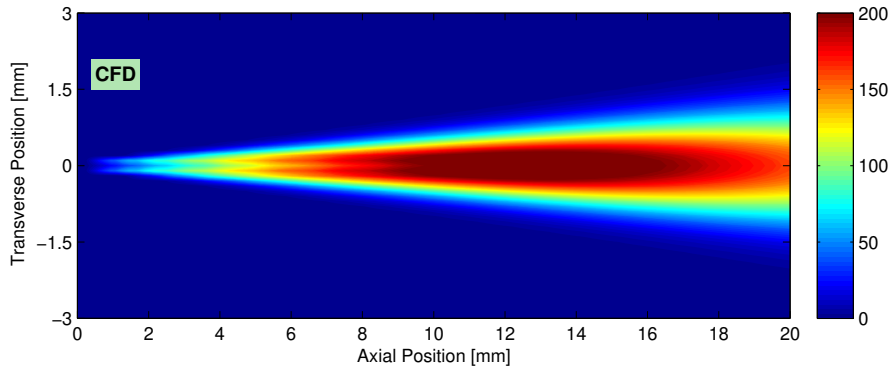

Figure 6. Contours of projected surface area [mm^2/mm^2] at 2.0 ms after SOI

density, as seen in Sec. 2, there are two model constants that should be calibrated due to their values are not fully established. This can be conducted by either using multiphase direct numerical simulation result, as in the studies from Demoulin et al.[16] and Duret et al.[35] or using a more straightforward approach, by means of the recent USAXS measurements[42]. This latter approach has been followed in this work.

Regarding α_1 constant, it has been shown at previous author$'s$ works[22,27,45] that this turbulent time-scale factor lies around one and has a limited impact on Σ equation predictions. However, α_2 parameter value shows a capital importance for modeling the interfacial surface density[27,45]. As previously mentioned, it is the inverse of the We_c for which values between 6 and 15 has been proposed by Chesnel et al.[46] from Diesel-like spray DNS[34]. Those two values where checked with the present Σ-Y model in Desantes et al.[45], and both overpredict projected surface area measurements for Spray A condition. Instead, fair agreement was found with $\alpha_2 = 0.035$, which corresponds to $We_c \sim$30. Then, this calibration is tested here for the Spray D condition as the initial guess. However, due to not completely satisfactory results, another configuration is simulated, see Table 6:

Table 6. Studies conducted for the calibration of the interface surface area equation parameters.

	α_1[-]	α_2[-]
Reference value	1.0	0.035
New value	1.0	0.02

In Fig. 7, radial profiles of projected surface area are shown at $2.0\ mm$, $6.0\ mm$ and $14.0\ mm$ downstream of the nozzle exit for both CFD predictions and USAXS measurements. Regarding the measurements, a local minimum in the projected surface area is observed at the spray centerline while two peaks appear at both sides. This minimum could be explained due to the presence of the intact liquid core at the

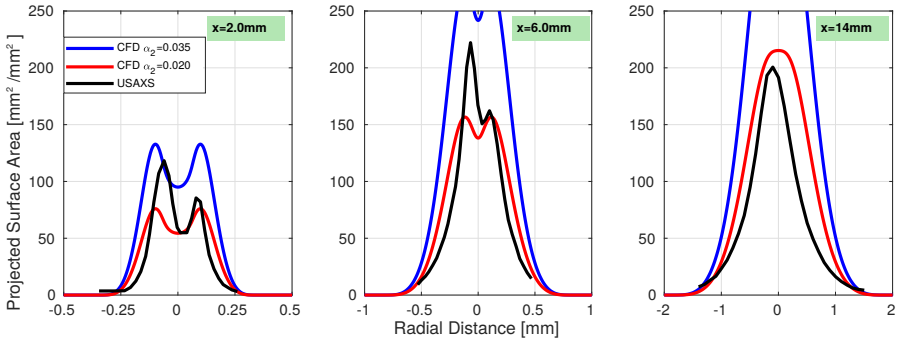

Figure 7. Computed and measured profiles of projected surface area [mm^2/mm^2] at 2.0 ms after SOI at axial locations of $2.0\ mm$, $6.0\ mm$, and $14.0\ mm$ downstream of the nozzle exit for different values of the second modeling constant

centerline, thus no interface should be present. Further downstream, this double-peak profile progressively vanishes, as can be seen at $x = 14.0\ mm$, and a normal gaussian -like one with the peak at the centerline is depicted. Modeling predictions reproduce extremely well the double-peak profile shape at first locations and even the transition to the gaussian one. However, it can be seen that with the Spray A reference configuration ($\alpha_2 = 0.035$), modeling results consistently overpredicts experimental peak data. New value ($\alpha_2 = 0.02$), can capture the value of one of the experimental peaks of the projected surface area while reproducing the gaussian profile at the last axial location ($14.0\ mm$). Additionally, in terms of modeling performance, in comparison with other interface modeling predictions (lagrangian, VOF-LES, VOF-DNS) shown recently in[44], quite remarkable results are shown at this work depicting heavily improved predictions in great agreement with the measurements.

Nevertheless, the difference in the optimum calibration for Spray D points out at some limitations in the Σ modelling approach. New α_2 value is almost two times (1.75) compared to previous calibration for Spray A[45], which was optimized based on-axis USASX available data, and for lower injection pressure(100 MPa) conditions. Indeed, some over-prediction for higher pressure (150 MPa) was found (see Fig. 13), so probably an intermediate value would be a compromise for both nozzles. Alternative formulations for Σ modelling[47] or adapted for LES turbulence framework[46] appears as paths for enhanced predictive capabilities, but they are out of the scope of the present contribution.

5.2 Spray D simulations under vaporizing conditions

After the successful assessment under cold conditions, vaporizing sprays are simulated. A time sequence of schlieren images and the corresponding simulated mass fraction contours are provided in Fig. 8 at several times during the spray development process. Note that due to the fact that CFD simulations are recorded every $5e^{-5}\ s$, small discrepancies between the experimental and the simulated times are shown. Nevertheless,

figure shows a good match in comparison with the measurements, in axial and radial extent.

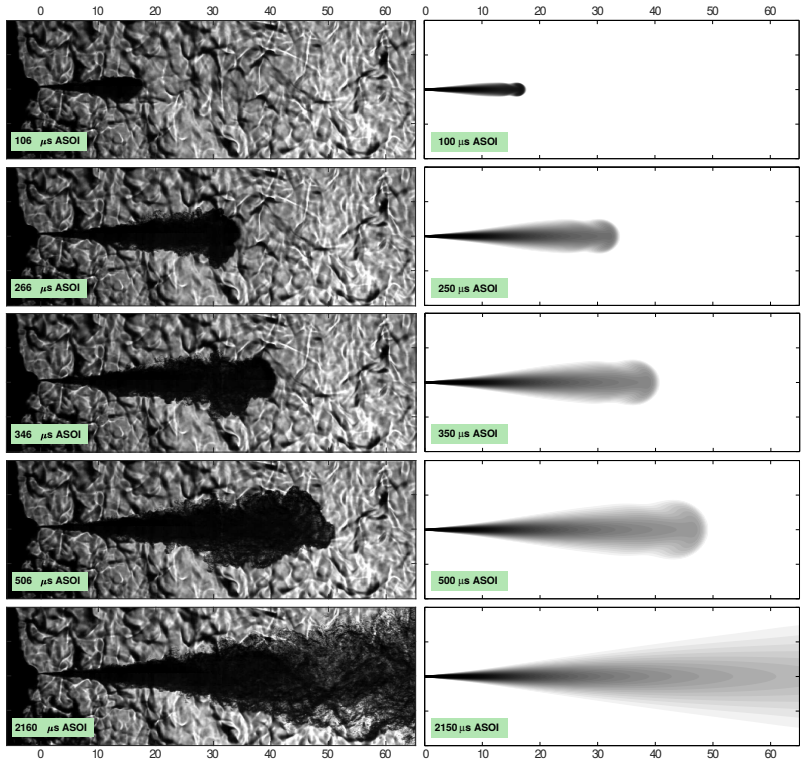

Figure 8. Spray images series seen by Schlieren (left) [36] and CFD prediction (right). Spray D, $P_{inj} = 150$ MPa, $\rho_{amb} = 22.8 kg/m^3$ and $T_{amb} = 900$ K

As explained at the experimental data section, a parametric study around the Spray D baseline condition is made, including different injection conditions as well as different ambient densities and temperatures. Then, in Fig. 9 to 11, spray vapor penetration and quasi-steady values of liquid length predictions have been summarized. Note that in the case of ambient temperature studies (Fig. 11), vapor penetration predictions are not shown because results present no departure among the different operating conditions, as it is controlled by the in nozzle momentum flux. Trends of decreasing vapor penetration with decreasing injection pressure and increasing or decreasing penetration when decreasing or increasing respectively ambient density are captured by the model. In general, good agreement between calculations and experiments is obtained, with predicted penetration results within experimental uncertainties.

In terms of quasi-steady values of liquid length, model exhibits good agreement, nearly matching the experimental measurements, keeping almost invariable predictions

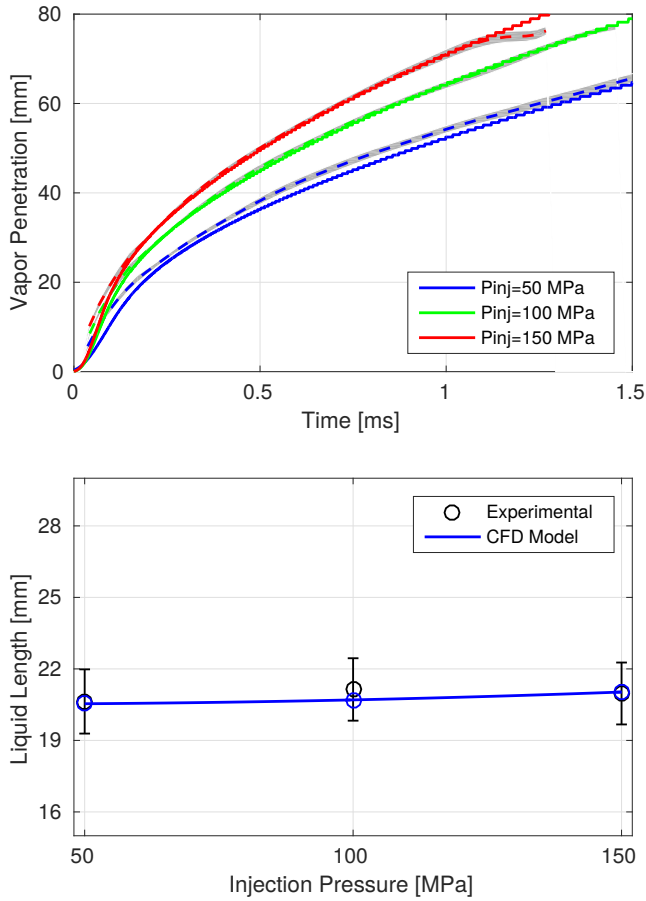

Figure 9. Computed (solid line) and measured (dotted line) spray tip penetration [top] and liquid length values [bottom] for different injection pressures. Spray D, $\rho_{amb} = 22.8kg/m^3$ and $T_{amb} = 900$ K

regarding the injection pressure. On the other hand, trends for different ambient density conditions are also well predicted. However, a slight departure (the model overpredicts the measurement in around a 10% for highest ambient density) appears as ambient gas density is increased. At the end, ambient temperature effects on quasi-steady values of liquid length are well reproduced, showing a maximum deviation with respect to the experimental measurements below 5%.

Overall, predictions always fall within the confidence interval of the measurements showing a remarkable modeling performance. Additionally, the accuracy in quasi-steady liquid length predictions supports that the evaporation process in wide range of diesel-like conditions is mainly mixing-controlled, as Siebers[12] concluded. The energy that

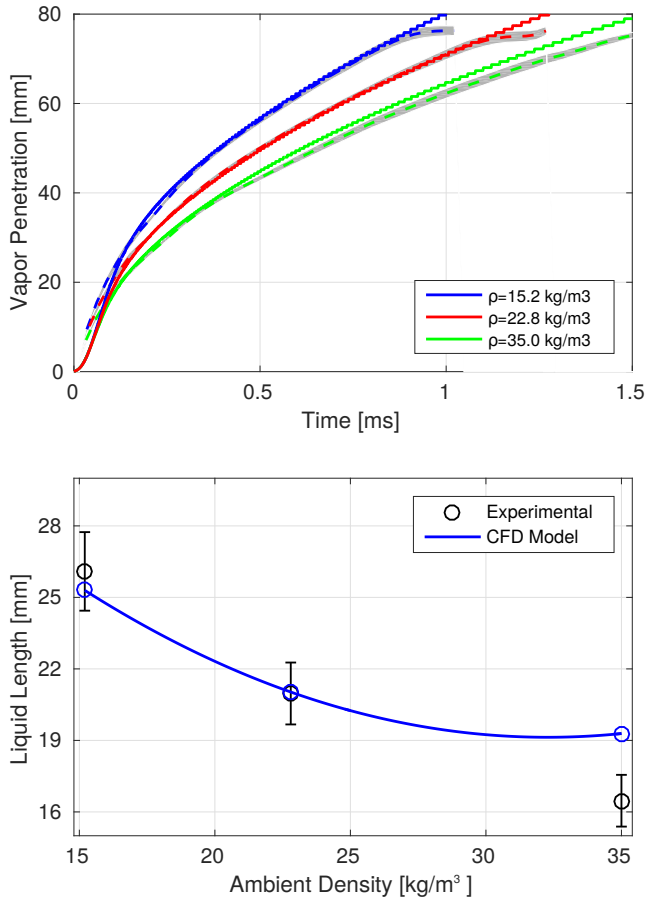

Figure 10. Computed (solid line) and measured (dotted line) spray tip penetration [top] and liquid length values [bottom] for different conditions of ambient density. Spray D, $P_{inj} = 150$ MPa and $T_{amb} = 900$ K

allows the fuel evaporation is transferred from the entrained air as a consequence of the turbulent mixing and therefore the liquid evaporates till reaching a characteristic mixture fraction.

5.3 Nozzle effects comparison on ECN Spray A and D

Finally, a comparison analysis between Spray A and Spray D modeling predictions is made. The interest of the discussion lies in evaluating the consistency of the model and the effects caused by the different nozzle geometry. As a result, similarly to the structure followed in the previous sections, the analysis begins with the spray structure in the near-nozzle region. In Fig. 12 transverse integrated mass profiles along the axis are

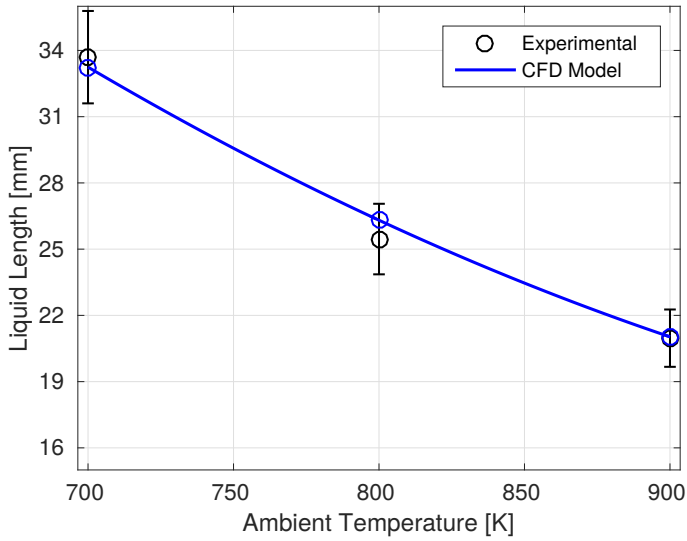

Figure 11. Computed and measured liquid length values for different conditions of ambient temperature. Spray D, $P_{inj} = 150$ MPa and $\rho_{amb} = 22.8kg/m^3$

presented for sprays A and D, both experimental and CFD ones. Note that two different charts are provided, the first one in which normalized spatial coordinates are used (left) and the second where both axis are normalized (right), with the respective scaling in terms of nozzle TIM value and equivalent diameter ($d_{eq} = d_0\sqrt{\rho_f/\rho_a}$). Results show a TIM level around four times greater in the case of Spray D, due to a bigger nozzle and corresponding injected fuel mass. However, more interesting is the axial evolution of the profile which could be analyzed without the impact of the nozzle size through the normalized horizontal coordinates. Spray D predictions are better than Spray A ones within the first $10\ mm$ (Fig. 5) downstream of the nozzle exit (near-nozzle region), but it is a consequence of the geometric characteristics. Here, one can observe that modeling predictions start to diverge from experimental measurements around $9 - 10\ d_{eq}$. In fact, focusing in Fig. 12 (right), Spray D mixes slightly faster than Spray A, but this is captured by the model which indicates that the trends are well reproduced.

Considering the effects on the atomization model, in Fig. 13 projected surface area profiles along the axis are evaluated. Note that experimental measurements for Spray D condition are only available within the first $14\ mm$ and also the different values of the α_2 modeling constant used, see Table 6:

In Fig. 13 (left), differences in the atomization proccess are depicted. Spray A condition presents a shorter liquid intact core and because of that the atomization process is located closer to the nozzle with the maximum of projected surface area located at around $6\ mm$ downstream of nozzle exit. Also, one can observe that Spray D shows

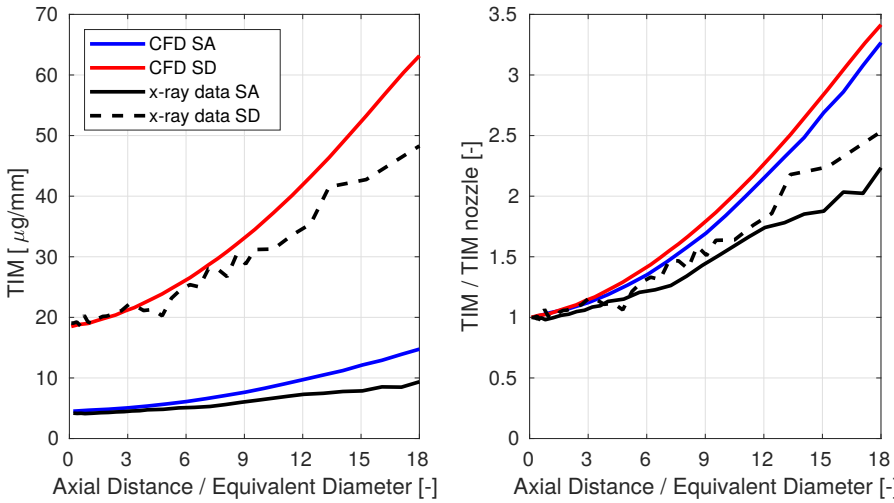

Figure 12. Computed and measured profiles of transverse integrated mass along the axis for Spray A and Spray D

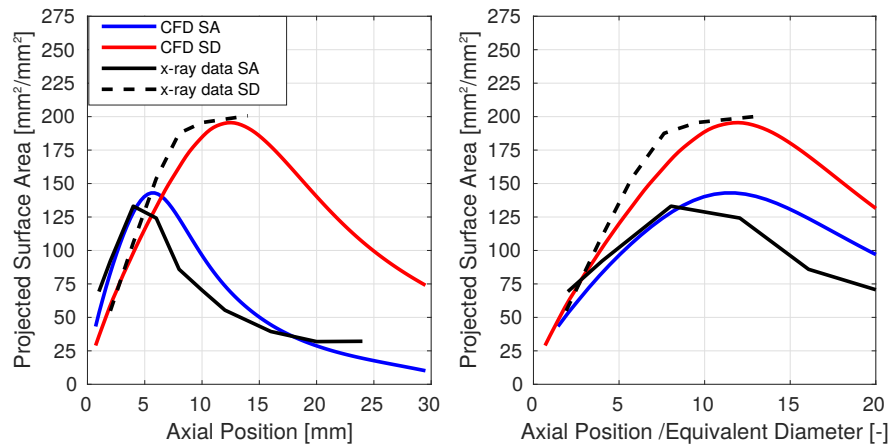

Figure 13. Computed and measured profiles of projected surface area [mm^2/mm^2] along the axis for Spray A and Spray D

a higher increase of the interface surface, due to a higher amount of fuel, reaching the maximum surface at a location around 12.5 mm downstream of nozzle exit, in accordance with double nozzle diameter. This is effectively checked in Fig. 13 (right), where the horizontal axis is normalized by the equivalent diameter. The maximum in projected surface area profiles is located at around 12 d_{eq} for both conditions. Finally, regarding the value of the α_2 modeling constant, calibration for the Spray A condition

was made based on the axial profile[45] and probably, as seen on this work, radial profiles give a more detailed information because of the double-peak shape. In any case, it is clear that with those calibrated values modeling performance is remarkable.

In terms of vaporazing sprays the analysis is conducted for the baseline condition, i.e. injection pressure $P_{inj} = 150$ MPa, ambient density $\rho_{amb} = 22.8kg/m^3$ and ambient temperature of $T_{amb} = 900$ K. In Fig. 14 (left), a comparison of the spray tip penetration as a function of time together with the the liquid length evolution is made. The figure is shown with normalized coordinates, penetration divided by the equivalent diameter and the non-dimensional time (t^*) as follows:

$$t^* = t\frac{U_0}{d_{eq}} \tag{11}$$

being t the time and U_0 the respective velocity at the nozzle exit.

According to the results, Spray A is seen to penetrate faster at the beginning with respect to Spray D and then, the acquired offset is kept constant for the complete spray evolution. This is a consequence of slightly faster initial ramp-up phase of the rate of injection for the smaller nozzle. On the other hand, equal normalized quasi-steady liquid lengths are provided indicating the linearity of this quantity with nozzle diameter.

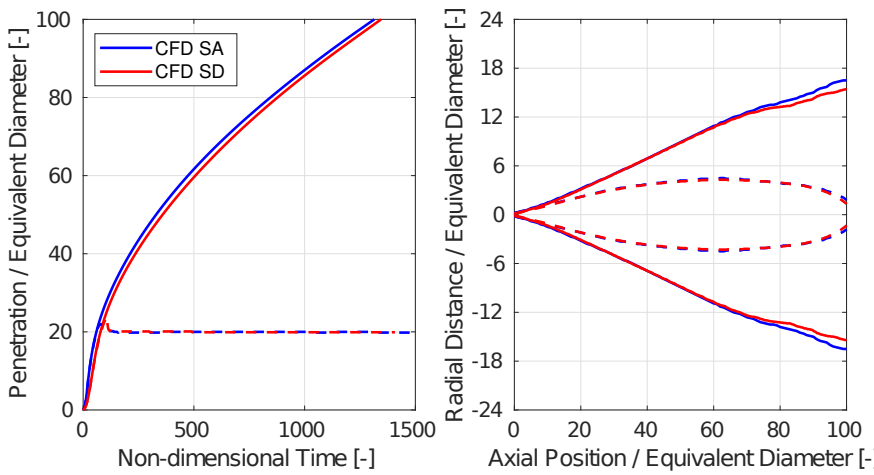

Figure 14. Computed spray tip penetration and liquid length [left] and contours of vapor region [right] for vaporizing Spray A and Spray D: Baseline, $P_{inj} = 150$ MPa , $T_{amb} = 900$ K and $\rho_{amb} = 22.8kg/m^3$

Spray vapor contours, Fig. 14 (right), are depicted for the same non-dimensional time (t^*), solid lines correspond to contours of 1% the on-axis mixture fraction value, while dashed lines show the stoichiometric iso-surface (considering an ambient with 21% of O_2 in molar basis). Mixture fields are equal under normalized coordinates, at the sight of stoichiometric iso-surfaces while spray contour is almost equal till around 70 d_{eq},

at this axial location Spray D countour begins narrower, as a result of the effect of the spray transient tip. Both penetration and spreading angle are closely related to air entrainment and mixing and thus, an analysis of the air entrainment process is made. Quantification of this parameter under Diesel engine conditions is not so common, but recent measurements shown by[48] and[49] have provided evaluation of entrainment rate for Spray A by means of PIV for both inert and reacting sprays, which will be analyzed here making use of CFD predictions. For that purpose, the entrainment coefficient is defined as

$$C_e(x) = \frac{d\dot{m}}{dx}\frac{d_{eq}}{\dot{m}_0} \tag{12}$$

where $\dot{m}$ is the mass flux across a full radial cross-section of the spray, $\dot{m}_0$ the mass flux at the orifice, x the downstream axial distance and d_{eq} the equivalent diameter. Then, entrainment rate is computed as a function of axial distance, considering that the spray radial limit is located at the radial position where the velocity is equal to 1% of the on-axis velocity.

$$\dot{m}(x) = \int \rho u \, dA = \int_0^R \rho u 2\pi r \, dr \tag{13}$$

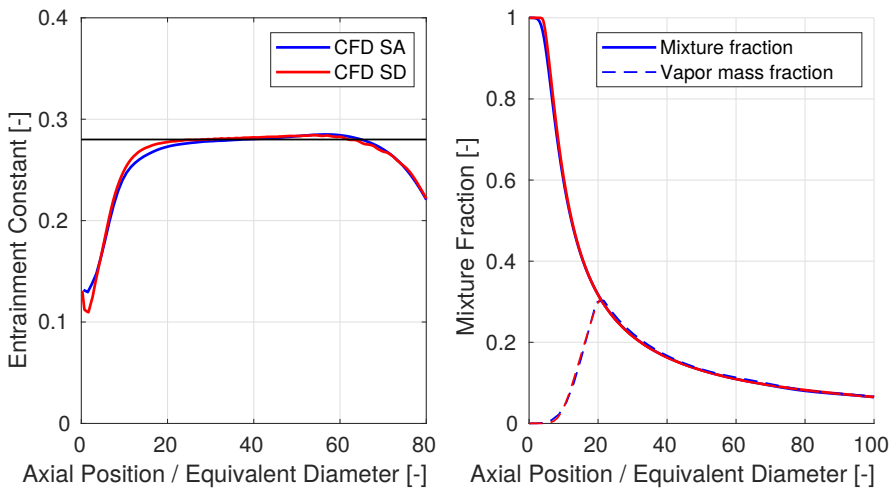

Figure 15. Computed entrainment constant [left], horizontal line indicates the 0.28 reference value derived from[48], and axial mixture fraction (solid line) and vapor mass fraction (dashed line) profiles [right] for vaporizing Spray A and Spray D: Baseline, $P_{inj} = 150$ MPa, $T_{amb} = 900$ K and $\rho_{amb} = 22.8 kg/m^3$

Computed local entrainment rate results are shown in Fig. 15 (left) for both conditions. Values have been averaged in an interval corresponding to the same non-dimensional times in order to ensure quasi-steady state predictions in a wide extension of the spray.

One can observe a transient region located near the nozzle (below 20 d_{eq}), where $C_e(x)$ has a lower value in agreement to results in[50,51] because of the transition between the nozzle flow and the fully developed turbulent spray. After that, a relatively flat evolution can be seen with a value quite near to the reference one of 0.28 derived in[48]. Lower values downstream 60 d_{eq} are a consequence of the effect of the transient tip of the spray, and because of that the horizontal axis of the figure is clipped downstream of 80 d_{eq}. Comparing both nozzles, simulations describe a similar behaviour with small differences located within the near-nozzle region. At the very nozzle exit, Spray D shows first a lower entrainment rate in agreement with the presence of the longer intact liquid core, which reaches around 5 d_{eq}. Further downstream, the entrainment of the larger nozzle along the near-nozzle region develops with a slightly higher mixing rate till 20 d_{eq}, in agreement with TIM results shown in Fig. 12 (right). However, when reaching the far-field region, where the spray flow is fully developed, entrainment rates of both nozzles are essentially the same. This means that both nozzles produce a very similar flow that scales with nozzle diameter, aside from local differences in the near-nozzle region. This result is consistent with computational studies from Post[52], which indicate that the effect of nozzle flow characteristics vanishes when reaching the fully-developed zone.

Finally, the previous discussion can be also held in terms of mixture fraction profiles. In Fig. 15 (right), the mixture fraction evolution on the spray axis for both sprays is presented together with the vapor mass fraction. All previous observations are confirmed with mixture fraction results. Previously described differences in intact liquid core are clearly shown in this figure. Further downstream, the slightly higher entrainment rate of Spray D recovers the initial lag in mixture fraction, and results in an overlap of the mixture fraction distribution with that of Spray A. Vapor mass fraction profiles are almost identical which leads to the same normalized liquid length shown in Fig. 14 (left).

6 Summary and Conclusions

The Σ-Y Eulerian atomization model has been applied to the study of direct injection diesel sprays from the ECN, sprays A and D, within a RANS turbulence modeling approach. Availability of recent measurements has made it possible to analyze the effect of a larger nozzle orifice on spray developemnt. CFD predictions are compared with previous results of Spray A in order to check the effects of the nozzle geometry on the modeling behaviour.

Nozzle flow, near- and far-field spray calculations have been performed for Spray D, both for non-vaporizing and vaporizing conditions. As a result, the validation is firstly made in terms of internal nozzle flow development by reproducing the value of the dimensionless coefficients. Model performance is quite accurate showing a maximum error with respect to experimental values lower than 4%. Additionally, some attention is paid to the internal structure of the spray at the near nozzle region. Validity of 2D decoupled simulations (in which the inlet boundary condition is taken from the coupled internal/external flow simulation) has been also confirmed for Spray D against x-ray radiography measurements of the non-vaporazing baseline condition of ECN, providing almost identical predictions as the coupled simulations in terms of projected mass density

and TIM. In comparison with experimental measurements, remarkable predictions has been shown within the first $10\ mm$ downstream of the nozzle exit. Regarding small scales features of the flow, a new calibration of the α_2 modeling constant for the interface surface model is performed. Radial profiles are evaluated being able to perfectly matched the double-peak shape shown at measurements independently of the constant value used.

For vaporizing conditions, predicted spray tip penetration and quasi-steady liquid lengths values have been evaluated through a parametric study around the Spray D baseline case. CFD predictions are in agreement with experimental data and only, in the case of higher ambient density, noticeable differences in terms of liquid length are depicted.

After the successful assessment of Spray D, the comparison with Spray A results is made. Under non-vaporizing conditions, although modeling general behaviour is quite similar, a slightly faster development of Spray D within $20\ d_{eq}$ has been found, evidenced by both modeling and experiments, which has been later confirmed under vaporizing conditions in terms of a slightly higher entrainment rate. Differences vanish in the fully-developed region downstream $20\ d_{eq}$.

In this work the overall applicability of the $\Sigma - Y$ modeling approach is confirmed by the validation studies. The predictive power of the model has been proved by using other injector nozzle and getting accurate results for internal flow together with the spray development and also under vaporizing conditions. Compared to previously shown configurations, only the α_2 constant value that defines the $\bar{\Sigma}_{eq}$ quantity for the surface area density model has been modified. This points out that Σ modelling approach should be further developed in order to enhance predictive capabilities.

Acknowledgements

Authors thank the freely shared X-ray radiography and Ultra-Small-Angle X-ray Scattering measurements performed at Argonne National Laboratory by the following authors: Daniel J. Duke, Jan Ilavsky, Katarzyna E. Matusik, Brandon A. Sforzo, Alan L. Kastengren, and Christopher F. Powell.

The authors thankfully acknowledges the computer resources at Picasso and the technical support provided by Universidad de Málaga (UMA) (RES-FI-2018-1-0039).

Declaration of conflicting interests

The author(s) declared no potential conflicts of interest with respect to the research, authorship, and/or publication of this article.

References

1. Payri R, García J, Salvador F et al. Using spray momentum flux measurements to understand the influence of diesel nozzle geometry on spray characteristics. *Fuel* 2005; 84(5): 551 – 561. DOI:http://dx.doi.org/10.1016/j.fuel.2004.10.009.
2. Payri R, Salvador F, Gimeno J et al. Diesel nozzle geometry influence on spray liquid-phase fuel penetration in evaporative conditions. *Fuel* 2008; 87(7): 1165 – 1176. DOI: http://dx.doi.org/10.1016/j.fuel.2007.05.058.

3. Payri R, Salvador F, Gimeno J et al. Effects of nozzle geometry on direct injection diesel engine combustion process. *Applied Thermal Engineering* 2009; 29(10): 2051 – 2060. DOI: http://dx.doi.org/10.1016/j.applthermaleng.2008.10.009.
4. Payri F, Payri R, Salvador F et al. A contribution to the understanding of cavitation effects in diesel injector nozzles through a combined experimental and computational investigation. *Computers & Fluids* 2012; 58: 88 – 101. DOI:https://doi.org/10.1016/j.compfluid.2012.01.005.
5. Kastengren AL, Tilocco FZ, Duke DJ et al. Time-resolved x-ray radiography of diesel injectors from the engine combustion network. *ICLASS Paper* 2012; (1369).
6. Kastengren AL, Powell CF, Wang Y et al. X-ray radiography measurements of diesel spray structure at engine-like ambient density. *Atomization and Sprays* 2009; 19(11): 1031–1044.
7. Pickett L, Manin J, Kastengren A et al. Comparison of near-field structure and growth of a diesel spray using light-based optical microscopy and x-ray radiography. *SAE Int J Engines* 2014; 7(2).
8. Dahms RN, Manin J, Pickett LM et al. Understanding high-pressure gas-liquid interface phenomena in diesel engines. *Proceedings of the Combustion Institute* 2013; 34(1): 1667 – 1675. DOI:http://dx.doi.org/10.1016/j.proci.2012.06.169.
9. Arienti M and Sussman M. A numerical study of the thermal transient in high-pressure diesel injection. *International Journal of Multiphase Flow* 2017; 88: 205 – 221. DOI: https://doi.org/10.1016/j.ijmultiphaseflow.2016.09.017.
10. Vallet A, Burluka A and Borghi R. Development of a Eulerian model for the "atomization" of a liquid jet. *Atomization and Sprays* 2001; 11: 619–642.
11. Siebers D. Liquid-phase fuel penetration in diesel sprays. *Trans SAE* 1998; 107: 1205–1227.
12. Siebers D. Scaling liquid-phase fuel penetration in diesel sprays based on mixing-limited vaporization. *Trans SAE* 1999; 108: 703–728.
13. Siebers DL. Recent developments on diesel fuel jets under quiescent conditions. In Arcoumanis C and Kamimoto T (eds.) *Flow and combustion in reciprocating engines*. Springer-Verlag, Berlin, 2008. pp. 257–308.
14. Oefelein J, Dahms R and Lacaze G. Detailed modeling and simulation of high-pressure fuel injection processes in diesel engines. *SAE Int J Engines* 2012; 5(3): 10.
15. Oefelein JC, Dahms RN, Lacaze G et al. Effects of pressure on the fundamental physics of fuel injection in diesel engines. *ICLASS Paper* 2012; .
16. Demoulin FX, Reveillon J, Duret B et al. Toward using direct numerical simulation to improve primary break-up modeling. *Atomization and Sprays* 2013; 23(11): 957–980.
17. Desantes JM, García-Oliver JM, Pastor JM et al. A comparison of diesel sprays CFD modelling approaches: DDM vs $\Sigma - Y$ eulerian atomization model. *Atomization and Sprays* 2016; 26(7): 713–737. DOI:10.1615/AtomizSpr.2015013285.
18. Desantes JM, García-Oliver JM, Pastor JM et al. Coupled / decoupled spray simulation comparison of the ECN spray a condition with the $\Sigma - Y$ eulerian atomization model. *International Journal of Multiphase Flow* 2016; 80: 89 – 99. DOI:http://dx.doi.org/10.1016/j.ijmultiphaseflow.2015.12.002.
19. García-Oliver JM, Pastor JM, Pandal A et al. Diesel spray CFD simulations based on the $\Sigma - Y$ eulerian atomization model. *Atomization and Sprays* 2013; 23: 71–95.

20. Navarro-Martinez S. Large eddy simulation of spray atomization with a probability density function method. *International Journal of Multiphase Flow* 2014; 63: 11 – 22. DOI: http://dx.doi.org/10.1016/j.ijmultiphaseflow.2014.02.013.
21. Pandal A, Pastor JM, García-Oliver JM et al. A consistent, scalable model for eulerian spray modeling. *International Journal of Multiphase Flow* 2016; 83: 162 – 171. DOI: http://dx.doi.org/10.1016/j.ijmultiphaseflow.2016.04.003.
22. Pandal A, Payri R, García-Oliver JM et al. Optimization of spray break-up CFD simulations by combining $\Sigma - Y$ eulerian atomization model with a response surface methodology under diesel engine-like conditions (ECN Spray A). *Computers & Fluids* 2017; 156: 9 – 20. DOI: https://doi.org/10.1016/j.compfluid.2017.06.022.
23. Pandal A, García-Oliver JM, Novella R et al. A computational analysis of local flow for reacting diesel sprays by means of an eulerian cfd model. *International Journal of Multiphase Flow* 2018; 99: 257 – 272. DOI:https://doi.org/10.1016/j.ijmultiphaseflow.2017.10.010.
24. Payri R, Ruiz S, Gimeno J et al. Verification of a new CFD compressible segregated and multi-phase solver with different flux updates-equations sequences. *Applied Mathematical Modelling* 2015; 39(2): 851 – 861. DOI:http://dx.doi.org/10.1016/j.apm.2014.07.011.
25. Salvador F, Gimeno J, Pastor J et al. Effect of turbulence model and inlet boundary condition on the diesel spray behavior simulated by an eulerian spray atomization (ESA) model. *International Journal of Multiphase Flow* 2014; 65: 108–116.
26. Demoulin F, Beau P, Blokkeel G et al. A new model for turbulent flows with large density fluctuations: application to liquid atomization. *Atomization and Sprays* 2007; 17: 315–345.
27. Pandal A, Pastor JM, Payri R et al. Computational and experimental investigation of interfacial area in near-field diesel spray simulation. *SAE Int J Fuels Lubr* 2017; 10. DOI: 10.4271/2017-01-0859.
28. ECN. Engine combustion network experimental data archive 2012; (accessed Nov 2018). URL http://www.sandia.gov/ecn/.
29. Weller H, Tabor G, Jasak H et al. A tensorial approach to computational continuum mechanics using object-oriented techniques. *Computers in Physics* 1998; 12: 620–631.
30. Reid R, Prausnitz J and Poling B. *The Properties of Gases and Liquids*. McGraw-Hill, 1987.
31. Faeth G. Evaporation and combustion of sprays. *Progress in Energy and Combustion Science* 1983; 9(1-2): 1–76. DOI:http://dx.doi.org/10.1016/0360-1285(83)90005-9.
32. Pitzer KS, Lippmann DZ, Jr RFC et al. The volumetric and thermodynamic properties of fluids. ii. compressibility factor, vapor pressure and entropy of vaporization1. *Journal of the American Chemical Society* 1955; 77(13): 3433–3440. DOI:10.1021/ja01618a002. http://dx.doi.org/10.1021/ja01618a002.
33. Vallet A and Borghi R. Modélisation Eulerienne de l'atomisation d'un jet liquide. *CR Acad Sci, Paris* 1999; 327: 1015–1020.
34. Lebas R, Menard T, Beau P et al. Numerical simulation of primary break-up and atomization: DNS and modeling study. *International Journal of Multiphase Flow* 2009; 35: 247–260.
35. Duret B, Reveillon J, Menard T et al. Improving primary atomization modeling through dns of two-phase flows. *International Journal of Multiphase Flow* 2013; 55: 130 – 137. DOI: https://doi.org/10.1016/j.ijmultiphaseflow.2013.05.004.
36. Gimeno J, Bracho G, Martí-Aldaraví P et al. Experimental study of the injection conditions influence over n-dodecane and diesel sprays with two ecn single-hole nozzles. part i: Inert

atmosphere. *Energy Conversion and Management* 2016; 126: 1146 – 1156. DOI:https://doi.org/10.1016/j.enconman.2016.07.077.

37. Kastengren A, Ilavsky J, Viera JP et al. Measurements of droplet size in shear-driven atomization using ultra-small angle x-ray scattering. *International Journal of Multiphase Flow* 2017; 92: 131 – 139. DOI:http://dx.doi.org/10.1016/j.ijmultiphaseflow.2017.03.005.
38. Kastengren A, Tilocco FZ, Powell CF et al. Engine combustion network (ECN):measurements of nozzle geometry and hydraulic behavior. *Atomization and Sprays* 2012; 22: 1011–1052.
39. Matusik KE, Duke DJ, Kastengren AL et al. High-resolution x-ray tomography of engine combustion network diesel injectors. *International Journal of Engine Research* 2018; 19(9): 963–976. DOI:10.1177/1468087417736985. https://doi.org/10.1177/1468087417736985.
40. Payri R, Gimeno J, Cuisano J et al. Hydraulic characterization of diesel engine single-hole injectors. *Fuel* 2016; 180: 357 – 366. DOI:https://doi.org/10.1016/j.fuel.2016.03.083.
41. Naber J and Siebers D. Effects of gas density and vaporization on penetration and dispersion of diesel sprays. *SAE Technical Paper* 1996; (960034). DOI:10.4271/960034.
42. ANL. X-Ray spray data archive, 2019. URL https://anl.app.box.com/v/XRaySpray.
43. Pope S. An explanation of the turbulent round-jet/plane-jet anomaly. *AIAA* 1978; 16: 279–281.
44. Battistoni M, Magnotti GM, Genzale CL et al. Experimental and computational investigation of subcritical near-nozzle spray structure and primary atomization in the engine combustion network spray d. *SAE Int J Fuels Lubr* 2018; 11: 337–352. DOI:10.4271/2018-01-0277.
45. Desantes JM, García-Oliver JM, Pastor JM et al. Modelling and validation of near-field diesel spray CFD simulations based on the $\Sigma - Y$ model. *ILASS Europe Paper* 2017; DOI:http://dx.doi.org/10.4995/ILASS2017.2017.4715.
46. Chesnel J, Reveillon J, Menard T et al. Large eddy simulation of liquid jet atomization. *Atomization and Sprays* 2011; 21(9): 711–736.
47. Devassy BM, Habchi C and Daniel E. Atomization modelling of liquid jets using a two-surface-density approach. *Atomization and Sprays* 2015; 25(1): 47–80.
48. Eagle W, Musculus M, Malbec L et al. Measuring transient entrainment rates of a confined vaporizing diesel jet. *ILASS Paper* 2014; .
49. García-Oliver JM, Malbec LM, Toda HB et al. A study on the interaction between local flow and flame structure for mixing-controlled diesel sprays. *Combustion and Flame* 2017; 179: 157 – 171. DOI:http://dx.doi.org/10.1016/j.combustflame.2017.01.023.
50. Han D and Mungal M. Direct measurement of entrainment in reacting/nonreacting turbulent jets. *Combustion and Flame* 2001; 124(3): 370 – 386. DOI:http://dx.doi.org/10.1016/S0010-2180(00)00211-X.
51. Hill BJ. Measurement of local entrainment rate in the initial region of axisymmetric turbulent air jets. *Journal of Fluid Mechanics* 1973; 51(4): 773779. DOI:doi:10.1017/S0022112072001351.
52. Post S AJ Iyer V. A study of near-field entrainment in gas jets and sprays under diesel conditions. *ASME J Fluids Eng* 1999; 122(2): 385–395. DOI:10.1115/1.483268.